

## Mathematical modelling of the residence time distribution of CO<sub>2</sub> tracer in a three-phase micro-packed bed reactor: An experimental analysis

Modelagem matemática da distribuição do tempo de residência do traçador de CO<sub>2</sub> em um reator trifásico de leito micro-empacotado: Uma análise experimental

Modelado matemática de la distribución del tiempo de residencia del trazador de CO<sub>2</sub> en un reactor de lecho micro-empacado trifásico: Un análisis experimental

Received: 06/21/2021 | Reviewed: 06/28/2021 | Accept: 07/15/2021 | Published: 07/25/2021

**José Marcelo da Silva**

ORCID: <https://orcid.org/0000-0002-6245-9576>  
University of Pernambuco, Brazil  
E-mail: [josemarcelo@eletronenergy.com.br](mailto:josemarcelo@eletronenergy.com.br)

**Vitória da Fonseca Dias**

ORCID: <https://orcid.org/0000-0001-6702-8962>  
University of Pernambuco, Brazil  
E-mail: [vi.dias11@hotmail.com](mailto:vi.dias11@hotmail.com)

**Jornandes Dias da Silva**

ORCID: <https://orcid.org/0000-0002-6346-1192>  
University of Pernambuco, Brazil  
E-mail: [jornandesdias@poli.br](mailto:jornandesdias@poli.br)

### Abstract

This study reports the residence time distribution (RTD) using CO<sub>2</sub> as tracer in Three-phase micro-packed bed (TP- $\mu$ PB) reactor. Experimental measurements were obtained at the inlet and at the outlet from TP- $\mu$ PB reactor using the injection of small amount (3%) of CO<sub>2</sub> tracer inside the sweep gas current. The dynamic model characterizes a diffusion-adsorption process of CO<sub>2</sub> tracer in terms of mass transfer phenomena (external and internal). The mathematical model was validated against a set of experimental data where simulated results of CO<sub>2</sub> tracer adequately matched the experimental measures at the outlet of the micro-packed bed.

**Keywords:** Experimental; Modelling; Reactor; Residence time; Tracer.

### Resumo

Este estudo descreve a distribuição do tempo de residência (DTR) usando CO<sub>2</sub> como um traçador no Reator Trifásico de Leito Micro-Empacotado (TL- $\mu$ E). As medições experimentais foram obtidas na entrada e na saída do reator TL- $\mu$ E usando a injeção de pequena quantidade (3%) do traçador de CO<sub>2</sub> dentro da corrente de gás de arraste. O modelo dinâmico caracteriza um processo de difusão-adsorção do traçador de CO<sub>2</sub> em termos de fenômenos de transferência de massa (externa e interna). O modelo matemático foi validado com base em um conjunto de resultados experimentais no qual os resultados simulados do traçador de CO<sub>2</sub> correspondem adequadamente às medidas experimentais na saída do leito micro-empacotados.

**Palavras-chave:** Experimental; Modelagem; Reator; Tempo de residência; Traçador.

### Resumen

Este estudio describe la distribución del tiempo de residencia (DTR) utilizando CO<sub>2</sub> como trazador en un reactor de lecho trifásico micro empaquetado (LT- $\mu$ E). Las mediciones experimentales fueron obtenidas a la entrada y salida del reactor de LT- $\mu$ E usando una pequeña cantidad de inyección (3%) del trazador de CO<sub>2</sub> en el interior de la corriente de gas portador. El modelo dinámico caracteriza un proceso de difusión-adsorción del trazador de CO<sub>2</sub> en términos de fenómenos de transferencia de masa (externo e interno). El modelo matemático fue validado en base a un conjunto de resultados experimentales en el que los resultados simulados del trazador de CO<sub>2</sub> coinciden adecuadamente a las mediciones experimentales a la salida del lecho micro-empacado.

**Palabras clave:** Experimental; Modelado; Reactor; Tiempo de residencia; Trazador.

## 1. Introduction

Three-phase micro-packed bed (TP- $\mu$ PB) reactors are an important and valuable device for process intensification where many applications are carried out with two or more immiscible fluids. When compared with conventional reactors, TP- $\mu$ PB reactors report several advantages, such as high surface-to-volume ratio and excellent mass and heat transfer performances (Anjos et al., 2019; Chen et al., 2016). These TP- $\mu$ PB reactor models of small catalyst (8-150 $\mu$ m) particles became efficient laboratory-tools in the case of heterogeneously catalyzed gas-liquid reactions (Anjos et al., 2017; Chang et al., 2003). The literature has investigated some works on heterogeneous catalytic process in micro-packed bed reactors for two phase and/or three phase systems (Cruz & Silva, 2017; Dias and Silva, 2020; Figueroa et al., 2018). These studies reported results of processes for liquid-solid and/or gas-liquid-solid systems using simple models, but authors did not provide guidance when TP- $\mu$ PB reactors have been used to a full mathematical model (equation for the gas phase, liquid phase and solid phase) (Bonfim et al., 2020; Gray et al., 2008; Kongnoo et al., 2017; Joss et al., 2017). We fill this gap with the concepts indicated by these authors and extend an application for the Residence Time Distribution (RTD) using CO<sub>2</sub> as tracer.

The analysis of the RTD from TP- $\mu$ PB reactor provides essential information about their overall performance (Silva, 2011, Moulijn et al., 2016). In addition, the RTD represents an useful tool in TP- $\mu$ PB reactor design, especially when deviations from ideal flow patterns (such as plug flow) play a key function in determining the reactor performance (Panariello et al. 2018; Silva et al., 2019). The RTD response is given by injecting a well-defined amount of the tracer into the inlet of TP- $\mu$ PB reactor at time  $t = 0$  and in turn recording the response of the tracer concentration at a central position of bed outlet.

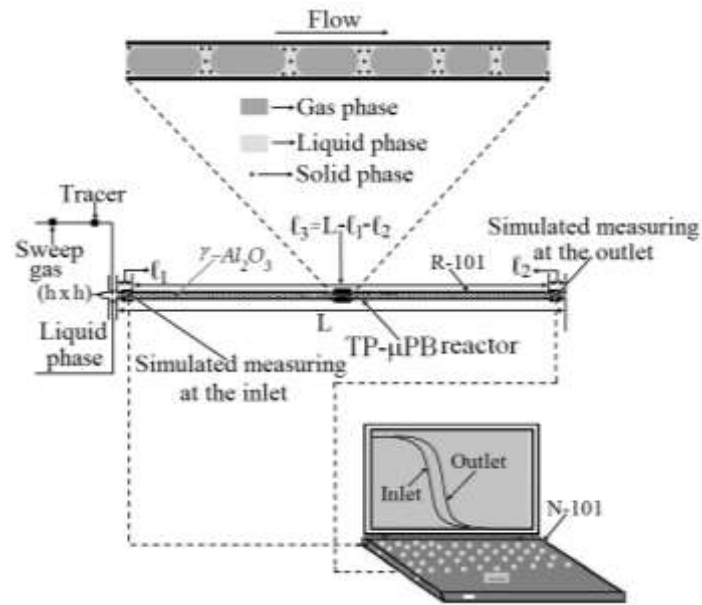
In this research, simulated measurements are carried out to study the RTD of CO<sub>2</sub> tracers in TP- $\mu$ PB reactor. A mathematical model is developed to compare the experimental results of the RTD with that simulated results from the mathematical model at the outlet from TP- $\mu$ PB reactor. The mathematical model is validated by minimizing the differences between the experimental and simulated measurements of the RTD of CO<sub>2</sub> tracer using as criterion an objective function.

## 2. Methodology

### 2.1 Problem characterization

The hydrodynamic characterization of the flow pattern through the micro-packed bed configuration in TP- $\mu$ PB reactor is carried out by tracing the main gaseous phase. A schematic diagram (SD) is shown to simulate the RTD experiments using the stimulus-response methodology. This SD is shown in Figure 1 as follows.

**Figure 1.** Schematic diagram for the experimental measurements.



Source: Authors.

The simulating protocol consists in the injection of CO<sub>2</sub> tracer into the major gaseous phase. The injection may not disturb the flow neither modify the physicochemical properties of the main gaseous phase. From the injection of CO<sub>2</sub> tracer, the concentration changes are simulated at the inlet and outlet from TP-μPB reactor according to Figure 1. The schematic setup from Figure 1 is constituted with a TP-μPB reactor (R-101), and notebook Dell (N-101, i155548-20, 1600 MHz (8GB), 1TB 5400 rpm), respectively. The heart from Figure 1 consists from a stainless steel TP-μPB reactor with the inner diameter of 0.5mm, the outer diameter of 0.9 mm and bed length of 0.6 m.

## 2.2 Working model from TP-μPB reactor

The governing equations of the developed mathematical model are described by mass balances limited to the region of the borders from TP-μPB reactor. In this work, the mass balance equations are developed based of CO<sub>2</sub> tracer in gas, liquid and solid phases. The developed mathematical model for CO<sub>2</sub> tracer within phases is restricted to the following simplifications: (i) isothermal system, (ii) the gas and liquid phases are modeled as plug flow, (iii) the system operates with partial wettability of solid particles, (iv) intraparticle diffusion in the pores of catalytic particles, (v) adsorption equilibrium in the system and (vi) the system operates with a small concentration of tracer in order to minimize disturbances in operating conditions from TP-μPB reactor. From above simplifications, the model equations can be described as follows.

## 2.3 Balance of CO<sub>2</sub> tracer in the gas phase

The mass balance equation of CO<sub>2</sub> tracer in the mobile gas phase inside TP-μPB reactor is composed by three terms (see Eq. 1). The first describes the transient term of CO<sub>2</sub> tracer, the second term expresses the convective mass flow towards the axial direction (z) in the gas phase, and the third term connects the gas-liquid mass transfer, respectively. All terms in Eq. 1 have unit of mol/m<sup>3</sup>sec. Thus, the mass balance of CO<sub>2</sub> tracer in the percolating mobile (gas) phase around the solid particles inside TP-μPB reactor is described as follows. The mass balance equation of CO<sub>2</sub> tracer in the mobile gas phase inside TP-μPB reactor is composed by three terms (see Eq. 1). The first describes the transient term of CO<sub>2</sub> tracer, the second term expresses the convective mass flow towards the axial direction (z) in the gas phase, and the third term connects the gas-liquid mass

transfer, respectively. All terms in Eq. 1 have unit of mol/m<sup>3</sup>sec. Thus, the mass balance of CO<sub>2</sub> tracer in the percolating mobile (gas) phase around the solid particles inside TP-μPB reactor is described as follows.

$$h_g \frac{\partial C_{CO_2,g}}{\partial t} + \frac{4q_g}{\pi d_\mu^2} \frac{\partial C_{CO_2,g}}{\partial z} = -k_{gl} a_{gl} \left( \frac{C_{CO_2,g}}{h_\mu} - C_{CO_2,l} \right) \quad (1)$$

In Equation (1),  $h_g$  (m<sup>3</sup>gas/m<sup>3</sup> reactor) is the gas holdup,  $t$  (sec.) is time,  $C_{CO_2,g}$  (kg/m<sup>3</sup>) is the molar concentration of CO<sub>2</sub> tracer in the gas phase,  $q_g$  (m<sup>3</sup>/sec.) is the gas flow rate in the gas phase,  $d_\mu$  (m) is the diameter from TP-μPB reactor,  $z$  (m) is the axial coordinate, respectively;  $k_{gl}$  (m/sec.) is the gas-liquid mass-transfer coefficient,  $a_{gl}$  (m<sup>2</sup>/ m<sup>3</sup> bed) is the gas-liquid mass-transfer area per unit column volume,  $h_\mu$  ( $C_{CO_2,g}/C_{CO_2,l}$ ) is the Henry's law solubility constant,  $C_{CO_2,l}$  (kg/m<sup>3</sup>) is the molar concentration of CO<sub>2</sub> tracer in the liquid phase, respectively.

The suitable initial and boundary conditions from Equation (1) are described as follows.

$$C_{CO_2,g} \Big|_{t=0, 1 \leq z \leq 3} = 0 \quad (2)$$

$$C_{CO_2,g} \Big|_{z=1, t \geq 0} = C_{CO_2,0} \quad (3)$$

$$C_{CO_2,g} \Big|_{z=3, t \geq 0} = C_{CO_2,\infty} \quad (4)$$

#### 2.4 Balance of CO<sub>2</sub> tracer in the liquid phase

The mass balance equation of CO<sub>2</sub> tracer in the mobile liquid phase within TP-μPB reactor is composed by four terms (see Eq. 5). The first describes the transient term of CO<sub>2</sub> tracer, the second term expresses the convective mass flow towards the axial direction ( $z$ ) in the liquid phase, the third term represents the gas-liquid mass transfer, and the fourth term connects the liquid-solid mass-transfer, respectively. All terms in Equation 3 have unit of mol/m<sup>3</sup>sec. Thus, the mass balance of CO<sub>2</sub> tracer in the percolating mobile (liquid) phase around the solid particles inside TP-μPB reactor is described as follows.

$$h_l \frac{\partial C_{CO_2,l}}{\partial t} + \frac{4q_l}{\pi d_\mu^2} \frac{\partial C_{CO_2,l}}{\partial z} = k_{gl} a_{gl} \left( \frac{C_{CO_2,g}}{h_\mu} - C_{CO_2,l} \right) - f_e k_{ls} a_{ls} \left( C_{CO_2,l} - C_{CO_2,p} \Big|_{r=R, t \geq 0} \right) \quad (5)$$

In Equation (5),  $h_l$  (m<sup>3</sup> dissolved gas in the liquid phase/m<sup>3</sup> reactor) is the dissolved gas holdup in the liquid phase,  $q_l$  (m<sup>3</sup>/sec.) is the gas flow rate in the liquid phase, respectively;  $f_e$  (-) is the wettability factor,  $k_{ls}$  (m/sec.) is the liquid-solid mass-transfer coefficient,  $a_{ls}$  (m<sup>2</sup>/m<sup>3</sup> bed) is the liquid-solid mass-transfer area per unit column volume,  $C_{i,p}$  (mol/m<sup>3</sup>) is the molar concentration of CO<sub>2</sub> tracer in the solid phase, respectively.

The suitable initial and boundary conditions from Equation (5) are described as follows.

$$C_{CO_2,l} \Big|_{t=0, 1 \leq z \leq 3} = 0 \quad (6)$$

$$C_{CO_2,l} \Big|_{z=1, t \geq 0} = 0 \quad (7)$$

$$C_{CO_2,l} \Big|_{z=1, t \geq 0} = C_{CO_2,l,\infty} \quad (8)$$

## 2.5 Balance of CO<sub>2</sub> tracer in the solid phase

Conceptually, CO<sub>2</sub> tracer is injected in the gas phase, dissolved in the liquid phase, and it is transferred towards the solid phase through the liquid film and then it diffuses in pores along the particle radius. The mass balance of CO<sub>2</sub> tracer inside the solid particle is given by three terms (see Eq. (9)). The first term reports the transient term of CO<sub>2</sub> tracer in pores of the solid particles, the second term describes the intraparticle diffusion of CO<sub>2</sub> tracer inside pores of the solid particles, the third term expresses the equilibrium adsorption of CO<sub>2</sub> tracer at the surface of the solid particles, respectively. All terms in Equation (9) have unit of mol/m<sup>3</sup>sec. Thus, the mass balance of CO<sub>2</sub> tracer in the solid particles is given as follows.

$$\varepsilon_s \frac{\partial C_{CO_2,p}}{\partial t} = \frac{D_{eff,CO_2}}{r^2} \frac{\partial}{\partial r} \left( r^2 \frac{\partial C_{CO_2,p}}{\partial r} \right) - \rho_p \left( k_{CO_2} C_{CO_2,p} + \frac{k_{CO_2}}{K_{CO_2}} C_{CO_2,ad} \right) \quad (9)$$

In Equation (9),  $h_s$  (m<sup>3</sup> dissolved gas in the solid phase/m<sup>3</sup> reactor) is the dissolved gas holdup in the solid phase,  $D_{eff,CO_2}$  (m<sup>2</sup>/sec.) is the diffusivity coefficient in pores of the solid particles,  $r$  (m) is the radial coordinate of the solid particles,  $\rho_p$  (mol/m<sup>3</sup>) is the density of the solid particles, respectively;  $k_{CO_2}$  (m<sup>3</sup>/mol sec.) is the adsorption rate constant,  $K_{CO_2}$  (m<sup>3</sup>/kg) is the adsorption equilibrium constant,  $C_{CO_2,ad}$  (mol/kg) is the concentration of tracer  $i$  at the surface of solid particles, respectively.

The suitable initial and boundary conditions from Equation (9) are reported as follows.

$$C_{CO_2,p} \Big|_{t=0, 0 \leq r \leq R} = 0 \quad (10)$$

$$\frac{\partial C_{CO_2,p}}{\partial r} \Big|_{r=R, t \geq 0} = \frac{k_{l,s}}{D_{eff,CO_2}} \left( C_{CO_2,l} - C_{CO_2,p} \Big|_{r=R, t \geq 0} \right) \quad (11)$$

$$\frac{\partial C_{CO_2,p}}{\partial r} \Big|_{r=0, t \geq 0} = 0 \quad (12)$$

## 2.6 Mass balance of CO<sub>2</sub> tracer at the surface of the solid phase

A mass balance equation has been proposed to describe the equilibrium adsorption rate of CO<sub>2</sub> tracer at the surface of the solid phase (Oliveira et al., 2020; Rios et al., 2014; Shen et al., 2011). The term  $(\partial C_{CO_2,ad}/\partial t)$  from Equation (7) describes the adsorbed amount of CO<sub>2</sub> tracer at the surface of the solid particles. All terms in Equation (13) have unit of mol/kg sec. The mass balance of CO<sub>2</sub> tracer at the surface of the particles is reported by Equation (13) as follows.

$$\frac{\partial C_{CO_2,ad}}{\partial t} = \rho_p k_{CO_2} C_{CO_2,p} - \left( \frac{k_{CO_2}}{K_{CO_2}} + k_r \right) C_{CO_2,ad} \quad (13)$$

The suitable initial condition from Equation (13) is reported as follows.

$$C_{CO_2,ad} \Big|_{t=0, r=R} = 0 \tag{14}$$

### 2.7 Solution of the mathematical modelling

The basic concept of the coupled integral equations approach (CIEA) can be given by the Hermite approximation and can be found in Ref. (Anjos et al., 2019). Thus, a general equation is reported as follows.

$$\int_{x_{i-1}}^{x_i} f(x)dx = \sum_{\nu=0}^{\alpha} c_{\nu}(\alpha, \beta) h_i^{\nu+1} f^{(\nu)}(x_{i-1}) + \sum_{\nu=0}^{\beta} c_{\nu}(\beta, \alpha) (-1)^{\nu} h_i^{\nu+1} f^{(\nu)}(x_i) + E_{\alpha, \beta} \tag{15}$$

Where,

$$h_i = x_i - x_{i-1}, c_{\nu}(\alpha, \beta) = \frac{(\alpha+1)!(\alpha+\beta-\nu+1)!}{(\nu+1)!(\alpha-\nu)!(\alpha+\beta+2)!} \tag{16}$$

The function  $f(x)$  and its derivatives  $f^{(\nu)}(x)$  are reported for all  $x \in [x_{i-1}, x_i]$ .  $E_{\alpha, \beta}$  is defined as the error in the approximation. In this context, it has been assumed that  $f^{(\nu)}(x_{i-1}) = f_i^{(\nu)}$  for  $\nu = 0, 1, 2, 3, \dots, \alpha$  and  $f^{(\nu)}(x_i) = f_i^{(\nu)}$  for  $\nu = 0, 1, 2, 3, \dots, \beta$ . As result, this integration formula can give different levels of approximation that are traditionally called of  $H_{\alpha, \beta}$ . Thus, approximations of order higher than  $H_{1,1}$  involve derivatives of order higher than one (Reis et al., 2018). These derivatives are avoided for the sake of simplicity of the methodology. Here, it was considered only two different approximations as follows.

$$H_{0,0} \rightarrow \int_0^h F(x)dx \approx \frac{1}{2}h \left[ F(x) \Big|_{x=0} + F(x) \Big|_{x=h} \right] \tag{17}$$

$$H_{1,1} \rightarrow \int_0^h F(x)dx \approx \frac{1}{2}h \left[ F(0) + F(h) \right] + \frac{1}{12}h^2 \left[ \frac{dF(x)}{dx} \Big|_{x=0} - \frac{dF(x)}{dx} \Big|_{x=h} \right] \tag{18}$$

In Equations (17) and (18),  $H_{0,0}$  is the trapezoidal integration rule,  $H_{1,1}$  is the corrected trapezoidal integration rule, respectively.

### 2.8 Application of the CIEA methodology

For solving the equations system, i.e., Equations (1)-(14) were resolved using the CIEA methodology. This methodology is used to transform EDPs into EDOs taking into account the boundary conditions. Here, it was used the expressions below to transform EDPs into EDOs in together with the boundary conditions.

$$\bar{F}_j(t) = \frac{1}{L_z} \int_0^{L_z} F_j(z,t) dz; j = g, l \text{ and } s \tag{19}$$

$$F_j(L_z, t) - F_j(0, t) \cong \frac{L_z}{2} \left[ \frac{\partial F_j(z,t)}{\partial z} \Big|_{z=0} + \frac{\partial F_j(z,t)}{\partial z} \Big|_{z=L_z} \right]; j = g, l \text{ and } s \tag{20}$$

$$\bar{F}_j(t) \cong \frac{L_z}{2} \left[ F_j(0,t) + F_j(L_z,t) \right] + \frac{L_z^2}{12} \left[ \left. \frac{\partial F_j(z,t)}{\partial z} \right|_{z=0} - \left. \frac{\partial F_j(z,t)}{\partial z} \right|_{z=L_z} \right]; j = g,l \text{ and } s \quad (21)$$

It is possible to transform the equations system, Equations (1)-(14), applying Equations (20)-(21) using the boundary conditions of each EDP (Medeiros et al., 2021). Thus, transformed equations are reported as follows.

$$h_g \frac{d\bar{C}_{CO_2,g}(t)}{dt} = k_{gl} a_{gl} \left[ h_\mu \bar{C}_{CO_2,l}(t) - \frac{1}{h_\mu} \bar{C}_{CO_2,g}(t) \right] \quad (22)$$

$$h_l \frac{d\bar{C}_{CO_2,l}(t)}{dt} = \frac{k_{gl} a_{gl}}{h_\mu} \bar{C}_{CO_2,g}(t) - (k_{gl} a_{gl} h_\mu + f_e k_{l,s} a_{l,s}) \bar{C}_{CO_2,l}(t) + f_e k_{l,s} a_{l,s} \bar{C}_{CO_2,p}(t) \quad (23)$$

$$\varepsilon_s \frac{d\bar{C}_{CO_2,p}(t)}{dt} = \alpha_{s,7} \bar{C}_{CO_2,p}(t) + \alpha_{s,8} \bar{C}_{CO_2,l}(t) - \frac{k_{CO_2}}{K_{CO_2}} \bar{C}_{CO_2,ad.}(t) + \alpha_{s,9} \bar{C}_{CO_2,l,\infty} \quad (24)$$

$$\frac{d\bar{C}_{CO_2,ad.}(t)}{dt} = \rho_p k_{CO_2} \bar{C}_{CO_2,p}(t) - \left( \frac{k_{CO_2}}{K_{CO_2}} + k_r \right) \bar{C}_{CO_2,ad.}(t) \quad (25)$$

All coefficients from Equations (22)-(25) are reported in equations below.

$$\alpha_{s,1} = \frac{R_p}{2} \left( 1 + \frac{R_p k_{l,s}}{6 D_{eff,CO_2}} \right); \alpha_{s,2} = \frac{R_p^2 k_{l,s}}{12 D_{eff,CO_2}}; \alpha_{s,3} = 1 + \frac{R_p k_{l,s}}{2 D_{eff,CO_2}}; \alpha_{g,4} = 1 + \frac{2\alpha_{g,1}}{R_p \alpha_{g,3}} \quad (26)$$

$$\alpha_{s,5} = \frac{1}{L_z \alpha_{g,3}} \left( \frac{4\alpha_{g,2}}{R_p} + \frac{R_p k_{l,s}}{D_{CO_2,eff}} \right); \alpha_{s,6} = \frac{1}{\alpha_{g,3}} \left( \frac{2\alpha_{g,2}}{R_p} + \frac{R_p k_{l,s}}{2D_{CO_2,eff}} \right) \quad (27)$$

$$\alpha_{s,7} = \rho_p k_{CO_2} - \frac{2}{R_p \alpha_{s,3} \alpha_{s,4}}; \alpha_{s,8} = \frac{2k_{l,s}}{L_z} - \frac{\alpha_{s,5}}{\alpha_{s,4}}; \alpha_{s,9} = \frac{\alpha_{s,6}}{\alpha_{s,4}} - k_{l,s} \quad (28)$$

## 2.9 Full solution's approximation

The choice of method is dependent on the desired accuracy as well as concerns about the stability and robustness of the system while maintaining computational efficiency. With respect to the transformed equations, Equations (22)-(25), they are solved by Runge-Kutta Gill method. Thus, the full solution is approximated using Equations (29)-(32) as follows.

$$C_{CO_2,g}(z,t) = \frac{1}{2} C_{CO_2,g}(z,t) \Big|_{t=0} + \sum_{k=1}^{\infty} \bar{C}_{CO_2,g}(t) \sin\left(\frac{k\pi z}{L_z}\right) \quad (29)$$

$$C_{CO_2,\ell}(z,t) = \frac{1}{2} C_{CO_2,\ell}(z,t) \Big|_{t=0} + \sum_{k=1}^{\infty} \bar{C}_{CO_2,\ell}(t) \sin\left(\frac{k\pi z}{L_z}\right) \quad (30)$$

$$C_{CO_2,p}(r,t) = \frac{1}{2} C_{CO_2,p}(r,t) \Big|_{t=0} + \sum_{k=1}^{\infty} \bar{C}_{CO_2,p}(t) \sin\left(\frac{k\pi r}{R_p}\right) \quad (31)$$

$$C_{CO_2,ad.}(r,t) = \frac{1}{2} C_{CO_2,ad.}(r,t) \Big|_{t=0} + \sum_{k=1}^{\infty} \bar{C}_{CO_2,ad}(r,t) \quad (32)$$

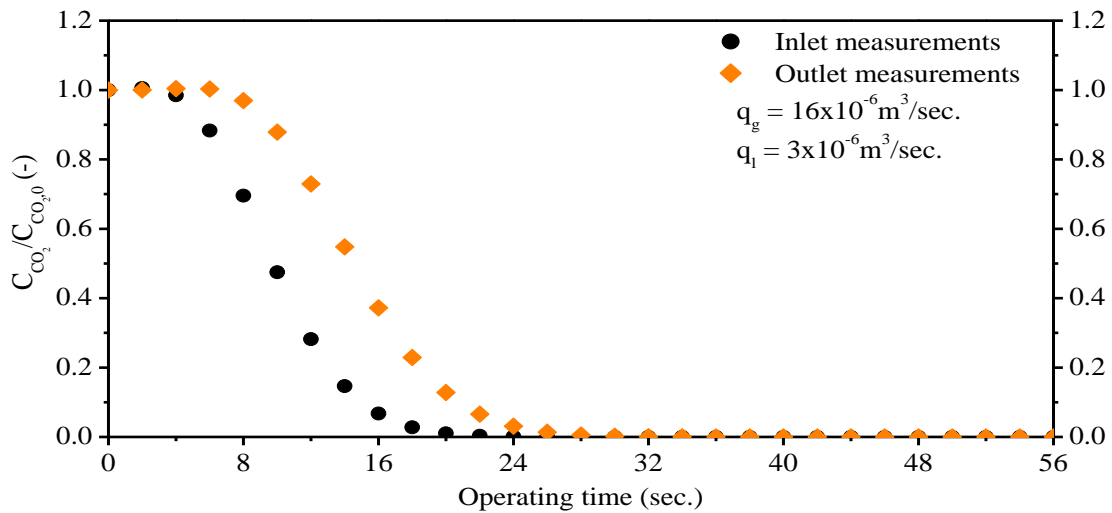
The experimental curves of CO<sub>2</sub> tracer are compared with the simulating curves obtained by the model equation described by the Equation (1) of the full model. A criterion was applied as indicator of the overall appropriateness of the adjustment for the experimental curves. This criterion has been defined as the sum of squared residuals (objective function (F<sub>of</sub>)) as follows.

$$F_{of} = \sum_{i=1}^{n_p} \left[ \left( C_{CO_2,g}/C_{CO_2,g,0} \right)_i^{Exp.} - \left( C_{CO_2,g}/C_{CO_2,g,0} f(C_{CO_2,\ell}, C_{CO_2,p}, C_{CO_2,ad.}) \right)_i^{Pred.} \right]^2 \quad (33)$$

### 3. Results and Discussions

The experimental results were measured at the inlet ( $\ell_1 = 0.05$ ) and outlet ( $\ell_3 = 0.95$ ) from micro-packed bed. As examples, Figure 2 shows the experimental RTD curves of CO<sub>2</sub> experimentally obtained for different flow rates (gas ( $16 \times 10^{-6} \text{ m}^3/\text{sec}$ ) and liquid ( $3 \times 10^{-6} \text{ m}^3/\text{sec}$ )) in terms of  $C_{CO_2}/C_{CO_2,0}$  versus time. In Figure 2, we show corresponding results of the injection of small amount (3%) of CO<sub>2</sub> tracer inside the sweep gas current. The operating temperature and operating pressure were kept constant at 300K in these experiments. From the injection of CO<sub>2</sub> tracer, the experimental measurements are obtained at the inlet and outlet from TP- $\mu$ PB reactor as function of the operating time.

**Figure 2.** Measurements of the concentration of CO<sub>2</sub> tracer at the inlet and at the outlet from TP- $\mu$ PB reactor.



Source: Authors.

#### 3.1 Model parameters for simulations

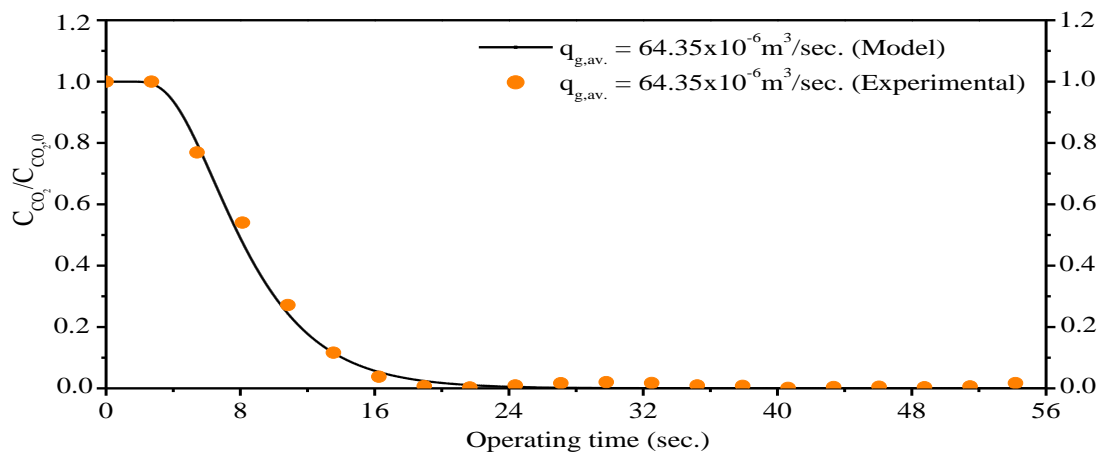
In Section 2, the coupled governing equations are described for tracer CO<sub>2</sub> in TP- $\mu$ PB reactor. In these equations, there are a parameter set that can be used to predict the simulated RTD curves. The inlet parameter values required for feeding the developed computational algorithm of this work are reported in Table 1. All these parameters (Table 1) are kept for same operating condition of this work.

**Table 1.** Reference parameters from the developed model used to simulate the experimental RTD curves of CO<sub>2</sub>.

Feed parameters	Values	References
$q_g$ (m <sup>3</sup> /sec.)	$64.35 \times 10^{-6} - 20.35 \times 10^{-6}$	Estimated
$q_l$ (m <sup>3</sup> /sec.)	$3.00 \times 10^{-6}$	Estimated
T (K)	300	Estimated
$P_{op}$ (kPa)	101	Estimated
$h_g$ (m <sup>3</sup> gas/m <sup>3</sup> reactor)	0.19	Estimated
$h_l$ (m <sup>3</sup> gas in liquid/m <sup>3</sup> reactor)	0.75	(Silva, 2011)
$d_\mu$ (m)	$1.8 \times 10^{-3}$	Estimated
$k_{gl}$ (m <sup>3</sup> bed/m <sup>2</sup> sec.)	$2 \times 10^{-4}$	(Silva, 2011)
$a_{gl}$ (m <sup>2</sup> / m <sup>3</sup> bed)	185	(Silva, 2011)
$h\mu$ (-)	$8.3 \times 10^{-1}$	Estimated
$\epsilon_p$ (m <sup>3</sup> gas/m <sup>3</sup> bed)	0.59	(Silva et al., 2019)
$D_{eff, CO_2}$ (m <sup>2</sup> /sec)	$1.87 \times 10^{-7}$	(Silva et al., 2019)
$f_{e,av}$ (-)	0.37	(Silva, 2011)
$k_{ts, av}$ (m <sup>3</sup> bed/m <sup>2</sup> sec.)	$4.63 \times 10^{-6}$	(Silva, 2011)
$\rho_p$ (kg/m <sup>3</sup> )	$2.56 \times 10^3$	(Silva, 2011)
$a_{ts}$ (m <sup>2</sup> / m <sup>3</sup> bed)	297	(Silva, 2011)
$L_z$ (mm)	16	Estimated
$k_{CO_2}$ (m <sup>3</sup> /kg sec.)	0.47	Estimated
$K_{CO_2}$ (kg/ m <sup>3</sup> )	$2.35 \times 10^3$	(Silva et al., 2019)
$k_r$ (sec. <sup>-1</sup> )	0.01	Estimated

Source: Authors.

**Figure 3.** Comparative analysis between the experimental and simulated measurements of the concentration of CO<sub>2</sub> tracer at the outlet from TP- $\mu$ PB reactor for  $q_{g,av} = 64.35 \times 10^{-6}$  m<sup>3</sup>/sec. and  $q_{l,av} = 3.0 \times 10^{-6}$  m<sup>3</sup>/sec.

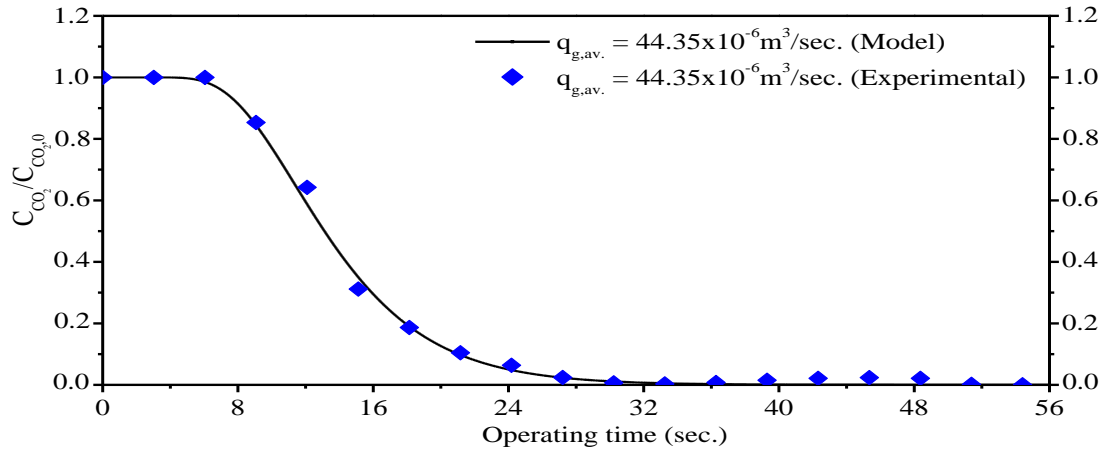


Source: Authors.

Figure 3 reports a comparative analysis between the experimental and simulated measures of the concentration of CO<sub>2</sub> tracer at the outlet from TP- $\mu$ PB reactor as function of the operating time. As seen from Figure 3, the simulated results are in

good agreement with experimental results obtained by Figure 1 with an objective function of  $F_{of} = 1.25 \times 10^{-4}$ . It is clear from this figure that as the flow rate increases the residence time decreases. Thus, the curves decrease at a faster operating time of more or less of 3.8 sec.

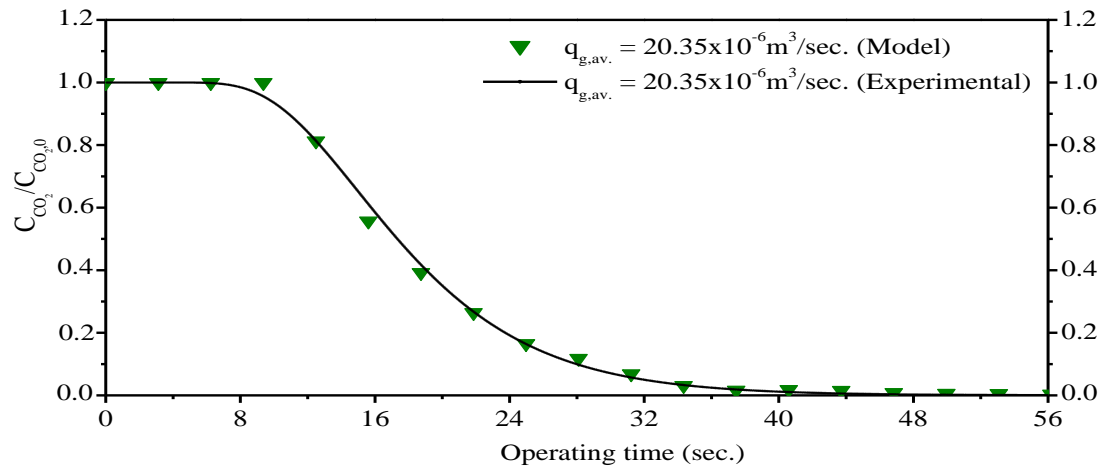
**Figure 4.** Comparative analysis between the experimental and simulated measurements of the concentration of  $CO_2$  tracer at the outlet from TP- $\mu$ PB reactor for  $q_{g,av.} = 44.35 \times 10^{-6} \text{ m}^3/\text{sec.}$  and  $q_{l,av.} = 3.0 \times 10^{-6} \text{ m}^3/\text{sec.}$



Source: Authors.

Figure 4 shows a comparative analysis between the experimental and simulated measures of the concentration of  $CO_2$  tracer at the outlet from TP- $\mu$ PB reactor as function of the operating time. From Figure 4, the simulated curves are in good adjustment with experimental curves obtained from Figure 1 with an objective function of  $F_{of} = 1.37 \times 10^{-4}$ . It is evident from this figure that for a smaller flow rate, the residence time increases. However, the curves decrease at a slower operating time of more or less of 6.3 sec.

**Figure 5.** Comparative analysis between the experimental and simulated measurements of the concentration of  $CO_2$  tracer at the outlet from TP- $\mu$ PB reactor for  $q_{g,av.} = 20.35 \times 10^{-6} \text{ m}^3/\text{sec.}$  and  $q_{l,av.} = 3.0 \times 10^{-6} \text{ m}^3/\text{sec.}$



Source: Authors.

Figure 5 presents a comparative analysis between the experimental and simulated measures of the concentration of  $CO_2$  tracer at the outlet from TP- $\mu$ PB reactor as function of the operating time. As from Figure 5, the simulated curves are in

good adjustment with experimental curves obtained from Figure 1 with an objective function of  $F_{of} = 2.09 \times 10^{-4}$ . In this figure, it becomes clearer that as the flow rate decreases the residence time increases. So, the curves decrease at an even slower operating time of more or less of 7.5 sec.

#### 4. Conclusion

A dynamics modelling coupled the adsorption isotherm that describes the distribution of CO<sub>2</sub> in TP- $\mu$ PB reactor was experimentally and numerically investigated. A computer code to simulate and validate the performance of the developed dynamic model for CO<sub>2</sub> tracer in TP- $\mu$ PB reactor allowed the following conclusions:

1. The Residence Time Distribution (RTD) curves of CO<sub>2</sub> tracer were experimentally obtained at the inlet and output of the micro-packed bed;
2. The experimental measures of CO<sub>2</sub> tracer at the three different flow rates are in good agreement with simulated results of the developed mathematical model;
3. The residence time of CO<sub>2</sub> tracer increases as the flow rate decreases.

As future works, novel tracers can be explored in the context to compute physical parameters. Moreover, new porous materials can be also used to improve the fluid-solid mass transfer. Solid open-cell foams consist in a kind of novel porous materials with low density and can be employed to enhance the mass absorption. On the other hand, solid open-cell foams are also used s potential candidates to generate efficiency products from chemical reactions.

#### Acknowledgments

The authors are grateful to University of Pernambuco for the financial support given (Project 127/2018).

#### References

- Anjos, E. B., Oliveira, C. B. & Silva, J. D. (2019). Dynamic analysis to produce hydrogen in a fixed bed catalytic reactor by the steam reforming of toluene. *Chemical Engineering Transactions*, 74, 553-558. <https://doi.org/10.3303/CET1974093>.
- Anjos, E. B., Carvalho, J. D. C. G. & Silva, J. D. (2017). Dynamic analysis of a three-phase reactor of fixed bed for petroleum and petrochemical industry. *In Proceedings of the 24th International Congress of Mechanical Engineering - COBEM 2017*, Curitiba, Brazil, 1-10.
- Anjos E. B. & Silva, J. D. (2019). Numerical simulation of the heat transfer for a three-phase reactor of fixed bed. *Latin IEEE Amer Trans*, 17, 788-795. <https://doi.org/10.1109/TLA.2019.8891947>.
- Bonfim, C. E. S., Pinto, J. C. C. S. & Poubel, W. M. (2020). CFD simulation for the analysis of a contaminated environment with chemical war: influence of flow profiles and determination of risk areas over a reservoir for water distribution. *Braz. J. of Develop.* 6, 25585-25608. <https://doi.org/10.34117/bjdv6n5-131>.
- Chang, A. C., Chuang, S. C., Gray, M. & Soong, Y. (2003). In-Situ Infrared Study of CO<sub>2</sub> Adsorption on SBA-15 Grafted with  $\gamma$ -(Aminopropyl) triethoxysilane. *Energy & Fuels*, 17, 468-473. <https://doi.org/10.1021/ef020176h>.
- Chen, S. J., Fu, Y., Huang, Y. X., Tao, Z. C. & Zhu, M. (2016). Experimental investigation of CO<sub>2</sub> separation by adsorption methods in natural gas purification. *Appl Energy*, 179, 329-337. <https://doi.org/10.1016/j.apenergy.2016.06.146>.
- Cruz, B. M. & Silva, J. D. (2017). A two-dimensional mathematical model for the catalytic steam reforming of methane in both conventional fixed-bed and fixed-bed membrane reactors for the Production of hydrogen. *Int J Hydrogen Energy*, 42, 23670-23690. <https://doi.org/10.1016/j.ijhydene.2017.03.019>.
- Dias, V. F. & Silva, J. D. (2020). Mathematical modelling of the solar-driven steam reforming of methanol for a solar thermochemical micro - fluidized bed reformer: thermal performance and thermochemical conversion. *J Braz Soc Mech Sci Eng*, 42, 447. <https://doi.org/10.1007/s40430-020-02529-6>.
- Figueroa, J. D., Fout, T., Plasynski, S., McIlvried, H. & Srivastava, R. D. (2018). Advances in CO<sub>2</sub> capture technology-The U.S. Department of Energy's Carbon Sequestration Program. *Int J Greenh Gas Control*, 2, 9-20. [https://doi.org/10.1016/S1750-5836\(07\)00094-1](https://doi.org/10.1016/S1750-5836(07)00094-1).
- Gray, M. L., Champagne, K. J., Fauth, D., Baltrus, J. P. & Pennline, H. (2008). Performance of immobilized tertiary amine solid sorbents for the capture of carbon dioxide. *Int. J. Greenh Gas Control*, 2, 3-8. [https://doi.org/10.1016/S1750-5836\(07\)00088-6](https://doi.org/10.1016/S1750-5836(07)00088-6).

- Joss, L., Gazzani, M. & Mazzotti, M. (2017). Rational design of temperature swing adsorption cycles for post-combustion CO<sub>2</sub> capture. *Chem Eng Sci*, 158, 709-716. <https://doi.org/10.1016/j.ces.2016.10.013>.
- Kongnoo, A., Tontisirin, S., Worathanakul, P. & Phalakornkule, C. (2017). Surface characteristics and CO<sub>2</sub> adsorption capacities of acid-activated zeolite 13X prepared from palm oil mill fly ash. *Fuel*, 193,385-394. <https://doi.org/10.1016/j.fuel.2016.12.087>.
- Medeiros, J. P. F., Dias, V. F., Silva, J. M. & Silva, J. D. (2021). Thermochemical Performance Analysis of the Steam Reforming of Methane in a Fixed Bed Membrane Reformer: A Modelling and Simulation Study. *Membranes*, 11, 6, 1-26. <https://doi.org/10.3390/membranes11010006>.
- Silva, J. D. (2011). Dynamic evaluation for liquid tracer in a trickle bed reactor. *Jour. Braz. Soc. Mech. Sci. Eng*, 33, 272-277. <https://doi.org/10.1590/S1678-58782011000300002>.
- Moulijn, J. A., Makkee M & Berger, R. J. (2016). Catalyst testing in multiphase micro-packed-bed reactors; criterion for radial mass transport. *Catal. Today*, 259, 354-359. <https://doi.org/10.1016/j.cattod.2015.05.025>.
- Oliveira, G. H. H., Oliveira, A. P. L. R., Souza, M. V. C., Neves, R. F. & Botelho, F. M. (2020). Water adsorption isotherms of coffee blends. *Braz. J. of Develop.*, 6, 20988-20997. <https://doi.org/10.34117/bjdv6n4-319>.
- Panariello, L., Mazzei, L. A. & Gavriilidis, A. (2018). Modelling the synthesis of nanoparticles in continuous microreactors: The role of diffusion and residence time distribution on nanoparticle characteristics. *Chem. Eng. Journal*, 350, 1144-1154. <https://doi.org/10.1016/j.cej.2018.03.167>.
- Rios, R. B., Correia, L. S., Bastos-Neto, M., Torres, A. E. B., Hatimondi, S. A., Ribeiro, A. M., Rodrigues, A. E., Cavalcante Jr, C. L. & de Azevedo, D. C. S. (2014). Evaluation of carbon dioxide-nitrogen separation through fixed bed measurements and simulations. *Adsorption*, 20, 945-957. <https://doi.org/10.1007/s10450-014-9639-3>.
- Shen, C., Yu, J., Li, P., Grande, C. A. & Rodrigues, A. E. (2011). Capture of CO<sub>2</sub> from flue gas by vacuum pressure swing adsorption using activated carbon beads. *Adsorption*, 17, 179-188. <https://doi.org/10.1007/s10450-010-9298-y>.
- Silva, P. B. A., Carvalho, J. D. C. G. & Silva, J. D. (2019). Hydrogen adsorption on Ni/γ-Al<sub>2</sub>O<sub>3</sub> in a fixed-bed adsorber: Experimental validation and numerical modelling. *Int J Hydrogen Energy*, 44, 304-317. <https://doi.org/10.1016/j.ijhydene.2018.07.203>.
- Reis, M. C., Sphaier, L. A., Alves, L. S. B. & Cotta, R. M. (2018). Approximate analytical methodology for calculating friction factors in flow through polygonal cross section ducts. *J Braz Soc Mech Sci Eng*, 40, 76. <https://doi.org/10.1007/s40430-018-1019-6>